Precision measurement of $\sigma(e^+e^- \to \pi^+\pi^-\gamma)/\sigma(e^+e^- \to \mu^+\mu^-\gamma)$ and determination of the $\pi^+\pi^-$ contribution to the muon anomaly with the KLOE detector

The KLOE and KLOE-2 Collaborations

D. Babusci [h], D. Badoni [r,s], I. Balwierz-Pytko [g], G. Bencivenni [h], C. Bini [p,q], C. Bloise [h], F. Bossi [h], P. Branchini [u], A. Budano [t,u], L. Caldeira Balkeståhl [w], G. Capon [h], F. Ceradini [t,u], P. Ciambrone [h], F. Curciarello [j,f], E. Czerwiński [h], E. Dané [h], V. De Leo [j,f], E. De Lucia [h], G. De Robertis [b], A. De Santis [p,q], P. De Simone [h], A. Di Domenico [p,q], C. Di Donato [ℓ,m], D. Domenici [h], O. Erriquez [a,b], G. Fanizzi [a,b], G. Felici [h], S. Fiore [p,q], P. Franzini [p,q], P. Gauzzi [p,q], G. Giardina [j,f], S. Giovannella [h], F. Gonnella [r,s], E. Graziani [u], F. Happacher [h], L. Heijkenskjöld [w], B. Höistad [w], L. Iafolla [h], E. Iarocci [n,h], M. Jacewicz [w], T. Johansson [w], W. Kluge [i], A. Kupsc [w], J. Lee-Franzini [h,v], F. Loddo [b], P. Lukin [h,ab], G. Mandaglio [j,f,e], M. Martemianov [k], M. Martini [h,o], M. Mascolo [r,s], R. Messi [r,s], S. Miscetti [h], G. Morello [h], D. Moricciani [s], P. Moskal [g], S. Müller [h,z], F. Nguyen [u,aa,*], A. Passeri [u], V. Patera [n,h], I. Prado Longhi [t,u], A. Ranieri [b], C. F. Redmer [w], P. Santangelo [h], I. Sarra [h], M. Schioppa [c,d], B. Sciascia [h], M. Silarski [g], C. Taccini [t,u], L. Tortora [u], G. Venanzoni [h,*], R. Versaci [h,y], W. Wiślicki [x], M. Wolke [w], J. Zdebik [g].

[a] Dipartimento di Fisica dell'Università di Bari, Bari, Italy.

[b] INFN Sezione Bari, Bari, Italy.

[c] Dipartimento di Fisica dell'Università della Calabria, Cosenza, Italy.

[d] INFN Gruppo collegato di Cosenza, Cosenza, Italy.

[e] Centro Siciliano di Fisica Nucleare e Struttura della Materia, Catania, Italy.

[f] INFN Sezione Catania, Catania, Italy.

[g] Institute of Physics, Jagiellonian University, Cracow, Poland.

[h]*Laboratori Nazionali di Frascati dell'INFN, Frascati, Italy.*

[i]*Institut fuür Experimentelle Kernphysik, Universität Karlsruhe, Germany.*

[j]*Dipartimento di Fisica e Scienze della Terra dell'Università di Messina, Messina, Italy.*

[k]*Institute for Theoretical and Experimental Physics (ITEP), Moscow, Russia.*

[ℓ]*Dipartimento di Fisica dell'Università "Federico II", Napoli, Italy.*

[m]*INFN Sezione Napoli, Napoli, Italy.*

[n]*Dipartimento di Scienze di Base ed Applicate per l'Ingegneria dell'Università "Sapienza", Roma, Italy.*

[o]*Dipartimento di Scienze e Tecnologie applicate, Università "Guglielmo Marconi", Roma, Italy.*

[p]*Dipartimento di Fisica dell'Università "Sapienza", Roma, Italy.*

[q]*INFN Sezione Roma, Roma, Italy.*

[r]*Dipartimento di Fisica dell'Università "Tor Vergata", Roma, Italy.*

[s]*INFN Sezione Roma Tor Vergata, Roma, Italy.*

[t]*Dipartimento di Fisica dell'Università "Roma Tre", Roma, Italy.*

[u]*INFN Sezione Roma Tre, Roma, Italy.*

[v]*Physics Department, State University of New York at Stony Brook, USA.*

[w]*Department of Physics and Astronomy, Uppsala University, Uppsala, Sweden.*

[x]*National Centre for Nuclear Research, Warsaw, Poland.*

[y]*Present Address: CERN, CH-1211 Geneva 23, Switzerland.*

[z]*Present Address: KVI, 9747 AA Groningen, The Netherlands.*

[aa]*Present Address: Laboratório de Instrumentação e Física Experimental de Partículas, Lisbon, Portugal.*

[ab]*Present Address: Budker Institute of Nuclear Physics, 630090 Novosibirsk, Russia.*

Abstract

We have measured the ratio $\sigma(e^+e^- \to \pi^+\pi^-\gamma)/\sigma(e^+e^- \to \mu^+\mu^-\gamma)$, with the KLOE detector at DAΦNE for a total integrated luminosity of $\sim$240 pb^{-1}. From this ratio we obtain the cross section $\sigma(e^+e^- \to \pi^+\pi^-)$. From the cross section we determine the pion form factor $|F_\pi(s)|^2$ and the two-pion contribution to the muon anomaly a_μ for $0.592 < M_{\pi\pi} < 0.975$ GeV, $\Delta^{\pi\pi}a_\mu = (385.1 \pm 1.1_{\text{stat}} \pm 2.7_{\text{sys+theo}}) \times 10^{-10}$. This result confirms the current discrepancy between the Standard Model calculation and the experimental measurement of the muon anomaly.

Key words: e^+e^- collisions, Initial state radiation, Pion form factor, Muon anomaly

13.40.Gp, 13.60.Hb, 13.66.De, 13.66.Jn

1 Introduction

Measurements of the muon magnetic anomaly $a_\mu = (g_\mu - 2)/2$ performed at the Brookhaven Laboratory have reached an accuracy of 0.54 ppm: $a_\mu = (11\,659\,208.0 \pm 6.3) \times 10^{-10}$ [1]. The quoted value differs from Standard Model estimates by 3.2-3.6 standard deviations [2–5] [1]. The difference between measurement and calculations is of great interest since it could be a signal of New Physics. The authors of Ref. 7 have proposed an interpretation in terms of Supersymmetry, which can be probed at the Large Hadron Collider. Another proposal suggests the existence of a light vector boson in the Dark Matter sector, coupled with ordinary fermions through photon exchange, which is not excluded by present low energy tests of the Standard Model [8, 9]. A new round of measurements of a_μ is expected at Fermilab [10] and J-PARC [11], with the aim of considerably reducing the experimental error. To fully exploit the significance of improved measurements of a_μ it is important to confirm the present estimate of the hadronic corrections (see below) and possibly to decrease the corresponding error.

The main source of uncertainty in the Standard Model estimates of a_μ [2, 3] is due to hadronic loop contributions which are not calculable in perturbative QCD. To lowest order, the hadronic contribution $\Delta^{\mathrm{h,\,lo}} a_\mu$, can be obtained from a dispersion integral [12, 13] over the "bare" cross section $\sigma^0(e^+ e^- \to \mathrm{hadrons}(\gamma))$. σ^0 is obtained from the physical cross section, inclusive of final state radiation, removing vacuum polarization, VP, effects and contributions due to additional photon emission in the initial state. The leading order hadronic contribution is $\sim 690 \times 10^{-10}$, the precise value depending on the authors' different averaging procedures, as discussed in Refs. 2–5. The $e^+ e^- \to \pi^+ \pi^-(\gamma)$ process contributes approximately 75% of the $\Delta^{\mathrm{h,\,lo}} a_\mu$ value and accounts for about 40% of its uncertainty.

In the following, we discuss the measurement of the cross sections as function of the $\mu^+ \mu^-$ and $\pi^+ \pi^-$ invariant masses $M_{\mu\mu}$ and $M_{\pi\pi}$:

$$\frac{\mathrm{d}\sigma(e^+ e^- \to \mu^+ \mu^- \gamma)}{\mathrm{d}s_\mu} \qquad \text{and} \qquad \frac{\mathrm{d}\sigma(e^+ e^- \to \pi^+ \pi^- \gamma)}{\mathrm{d}s_\pi}$$

with $s_\mu = M_{\mu\mu}^2$, $s_\pi = M_{\pi\pi}^2$, to be used for the determination of $\sigma^0(e^+ e^- \to \pi^+ \pi^-)$. From the latter we obtain the two-pion contribution to the anomaly, $\Delta^{\mathrm{h,\,lo}} a_\mu$ and the pion form factor $|F_\pi|^2$ for comparison to other results.

---

* Corresponding authors.
  Email addresses: `federico.nguyen@cern.ch` (F. Nguyen),
`graziano.venanzoni@lnf.infn.it` (G. Venanzoni).
[1] A recent evaluation [6] finds a difference between 4.7 and 4.9 standard deviations.

2 Measurement of $\sigma(\pi^+\pi^-)$ at DAΦNE

The KLOE detector operates at DAΦNE, the Frascati ϕ–factory, an e^+e^- collider running at fixed energy, $W = \sqrt{s} \sim 1020$ MeV, the ϕ meson mass. Initial state radiation (ISR) provides a means to produce $\pi^+\pi^-$ pairs of variable s_π. Counting $\pi^+\pi^-\gamma$ events leads to a measurement of $\mathrm{d}\sigma(e^+e^- \to \pi^+\pi^-\gamma)/\mathrm{d}s_\pi$ if the integrated luminosity is known, from which $\sigma(e^+e^- \to \pi^+\pi^-)$ can be extracted. We have published three measurements [14–16] of $\sigma(e^+e^- \to \pi^+\pi^-)$ for $0.1 < M_{\pi\pi}^2 < 0.95$ GeV^2, with results consistent within errors and a combined fractional uncertainty of about 1%. The luminosity was obtained by counting Bhabha scattering events and using the QED value of the corresponding cross section. To lowest order, the pion form factor is defined by:
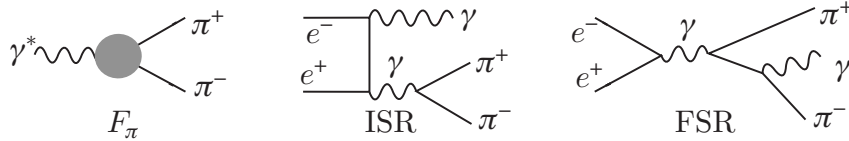

Fig. 1. Simplified amplitudes for $\gamma^* \to \pi^+\pi^-$, $e^+e^- \to \pi^+\pi^-\gamma$ (ISR) and $e^+e^- \to \pi^+\pi^-\gamma$ (FSR).

$$\langle \pi^+\pi^- | J_\mu^{\mathrm{em}}(\pi) | 0 \rangle = (p_+ - p_-)_\mu \times F_\pi \left(s_\pi = (p_+ + p_-)^2 \right). \tag{1}$$

The differential cross section for $e^+e^- \to \pi^+\pi^-\gamma$ due to the ISR amplitude of Fig. 1 is related to the dipion cross section $\sigma_{\pi\pi} \equiv \sigma(e^+e^- \to \pi^+\pi^-\gamma)$ [17]:

$$s \left. \frac{\mathrm{d}\sigma(\pi^+\pi^-\gamma)}{\mathrm{d}s_\pi} \right|_{\mathrm{ISR}} = \sigma_{\pi\pi}(s_\pi) \, H(s_\pi, s), \tag{2}$$

where the radiator function H is computed from QED with complete NLO corrections [18–22] and depends on the e^+e^- center of mass energy squared s. $\sigma_{\pi\pi}$ obtained from Eq. 2 requires accounting for final state radiation (FSR in Fig. 1). In the following we only use events where the photon is emitted at small angle, as discussed in detail in Refs. 15,16. The cross section for $e^+e^- \to \pi^+\pi^-\gamma$ is proportional to the two-photon e^+e^- annihilation cross section, which diverges, at lowest order, for the photon angle going to zero. This is not the case for the FSR contribution. Our choice results in a large enhancement of ISR with respect to FSR contribution.

Equation 2 is also valid for $e^+e^- \to \mu^+\mu^-\gamma$ and $e^+e^- \to \mu^+\mu^-$ with the same radiator function H. We can therefore determine $\sigma_{\pi\pi}$ from the ratio of the $\pi^+\pi^-\gamma$ and $\mu^+\mu^-\gamma$ differential cross sections for the same value of the dipion

and dimuon invariant mass. For ISR events we have:

$$\sigma^0(\pi^+\pi^-, \ s') = \frac{d\sigma(\pi^+\pi^-\gamma, \ \text{ISR})/ds'}{d\sigma(\mu^+\mu^-\gamma, \ \text{ISR})/ds'} \times \sigma^0(e^+e^- \to \mu^+\mu^-, \ s'). \quad (3)$$

where $s' = s_\pi = s_\mu$.

Final state photon emission for both the $\pi^+\pi^-\gamma$ and $\mu^+\mu^-\gamma$ channels slightly modifies Eq. 3. These corrections are included in our analysis [23].

From the bare cross section $\sigma^0_{\pi\pi}$ we obtain the pion form factor:

$$|F_\pi(s')|^2 = \frac{3}{\pi} \frac{s'}{\alpha^2 \beta_\pi^3} \ \sigma^0_{\pi\pi(\gamma)}(s')(1 + \delta_{VP})(1 - \eta_\pi(s')) \quad (4)$$

where δ_{VP} is the VP correction [24] and η_π accounts for FSR radiation assuming point-like pions [25].

The advantages of the ratio method are:

(1) the H function does not appear in Eq. 3. Therefore the measurement of $\sigma_{\pi\pi}$ is not affected by the related systematic uncertainty of 0.5% [18] ;
(2) using the same data sample for the $\pi^+\pi^-\gamma$ and $\mu^+\mu^-\gamma$ events, there is no need for luminosity measurements;
(3) vacuum polarization corrections and most other radiative corrections cancel in the ratio;
(4) using the same fiducial volume, acceptance corrections to the $\pi^+\pi^-\gamma$ and $\mu^+\mu^-\gamma$ spectra almost cancel resulting in a small systematic uncertainty.

In the following we describe the measurement of $d\sigma_{\mu\mu\gamma}/ds_\mu$ using the same data used to measure $d\sigma_{\pi\pi\gamma}/ds_\pi$ [15].

3 Measurement of the $e^+e^- \to \mu^+\mu^-\gamma$ cross section

The data sample corresponds to an integrated luminosity of 239.2 pb^{-1} collected in 2002, with low machine background and stable DAΦNE conditions. We also recorded events without offline filters with a down scaled trigger, providing control samples for evaluating efficiencies.

3.1 The KLOE Detector

The KLOE detector consists of a cylindrical drift chamber (DC) [26] and a lead–scintillating fibers electromagnetic calorimeter (EMC) [27]. The DC has a momentum resolution of $\sigma_{p_\perp}/p_\perp \sim 0.4\%$ for tracks with polar angle $\theta > 45°$. Track points are measured in the DC with a resolution in r-ϕ of about 0.15 mm and about 2 mm in z. The EMC has an energy resolution of $\sigma_E/E \sim 5.7\%/\sqrt{\text{E (GeV)}}$ and an excellent time resolution of $\sigma_t \sim 57$ ps$/\sqrt{\text{E (GeV)}} \oplus 100$ ps. A cross section of the detector in the y, z plane is shown in Fig. 2. A superconducting coil provides an axial magnetic field of 0.52 T along
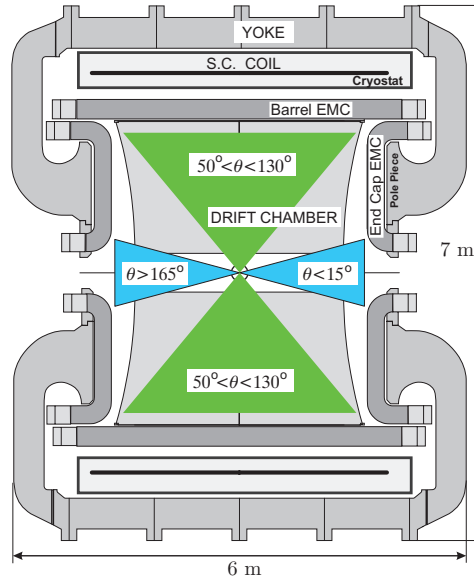

Fig. 2. Vertical cross section of the KLOE detector, showing the small and large angle regions where respectively photons and muons are accepted

the bisector of the colliding beam directions. The bisector is taken as the z axis of our coordinate system. The x axis is horizontal, pointing to the center of the collider rings and the y axis is vertical, directed upwards. The trigger [28] uses both EMC and DC information. Events used in this analysis are triggered by two energy deposits larger than 50 MeV in two sectors of the barrel calorimeter.

3.2 Identification of $e^+e^- \to \mu^+\mu^-\gamma$ events

The signature for $e^+e^- \to \mu\mu\gamma$ events with the photon emitted at small angle is just two tracks of opposite curvature, the photon being lost in the beam pipe. Four types of events contribute to the above signatures: 1: $e^+e^- \to \mu\mu\gamma$, 2: $e^+e^- \to \pi^+\pi^-\gamma$, 3: $e^+e^- \to e^+e^-\gamma$, and 4: $e^+e^- \to \pi^+\pi^-\pi^0$. The four reactions can be distinguished kinematically. From the reaction $e^+e^- \to x^+x^-\gamma$, which is

6

once kinematically overconstrained, we can compute the common mass $(m(x))$ of particles x^+ and x^-. The four processes give $m(x) = m_\mu$, m_π, m_e and $> m_\pi$. Additional separation between electrons and pions or muons is obtained from a particle identification (PID) estimator for each track, $L_\pm$, which uses time of flight information and the value and shape of the energy deposit of each charged particle in the calorimeter [15]. Figure 2 shows the fiducial volume we use for muons and unobserved photons which is identical to that used in Ref. 15 for $e^+e^- \to \pi^+\pi^-\gamma$.

We list below the requirements for event acceptance.

(1) Events must have at least two tracks of opposite sign, with origin at the interaction point and polar angle satisfying $50° < \theta < 130°$. The reconstructed momenta must satisfy $p_\perp > 160$ MeV or $|p_z| > 90$ MeV, to ensure good reconstruction and efficiency.
(2) The polar angle $\theta_{\mu\mu}$ of the the dimuon system obtained from the momentum of the two tracks $(\mathbf{p}_{\mu\mu} = \mathbf{p}_+ + \mathbf{p}_-)$ must satisfy $|\cos\theta_{\mu\mu}| > \cos(15°)$.
(3) Events with both tracks having $L_\pm < 0$ are identified as $ee\gamma$ events and rejected. The loss due to this cut is less than 0.05%, as evaluated with $\mu\mu$ samples, obtained from both data and Monte Carlo.
(4) The computed mass for the two observed particles must satisfy $80 < m_x < 115$ MeV.

About 8.9×10^5 events pass these criteria. Figure 3 shows the m_x distribution together with the accepted regions for $\mu\mu\gamma$ and $\pi\pi\gamma$ events [15].
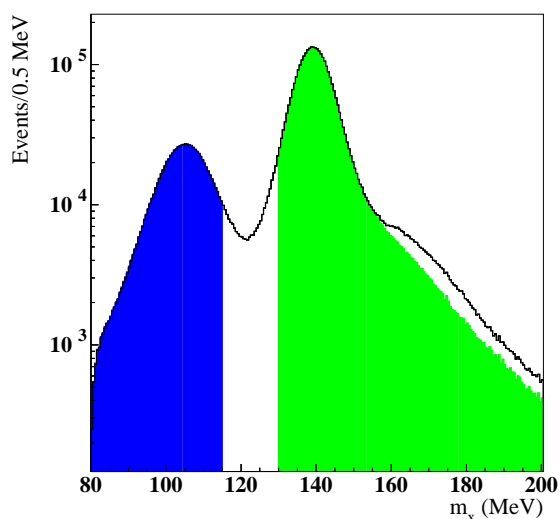

Fig. 3. Data $\mu\mu\gamma$ and $\pi\pi\gamma$ regions in the m_x spectrum. The $\mu\mu\gamma$ and $\pi\pi\gamma$ accepted regions are shown in in blue and green. A residual contamination of $\pi^+\pi^-\pi^0$ events is visible at high m_x values.

3.3 Background estimates

Residual $e^+e^-\gamma$, $\pi^+\pi^-\gamma$ and $\pi^+\pi^-\pi^0$ backgrounds are evaluated by fitting the observed m_x spectrum with a superposition of Monte Carlo simulation (MC) distributions describing signal and $\pi^+\pi^-\gamma$, $\pi^+\pi^-\pi^0$ backgrounds, and a distribution obtained from data for the $e^+e^-\gamma$ background. The normalized contributions from signal and backgrounds are free parameters of the fit, performed for 30 intervals in $M_{\mu\mu}^2$ of 0.02 GeV^2 width for $0.35 < M_{\mu\mu}^2 < 0.95$ GeV^2.

In the ρ mass region, the fractional $\pi^+\pi^-\gamma$ yield in the $\mu\mu\gamma$ acceptance region is about 15% of the sample. To improve the MC description of the low energy m_x tail of $\pi^+\pi^-\gamma$ events in the muon peak, Fig. 3, we apply a data/MC resolution correction, function of s_μ. This correction is evaluated from a high purity sample of $\phi \rightarrow \pi^+\pi^-\pi^0$ events, with the same track requirements used for $\mu\mu\gamma$ events, requiring in addition two photons with an invariant mass compatible with the π^0 mass, both for data and MC. Figure 4 shows the comparison between data and MC before and after the resolution correction.
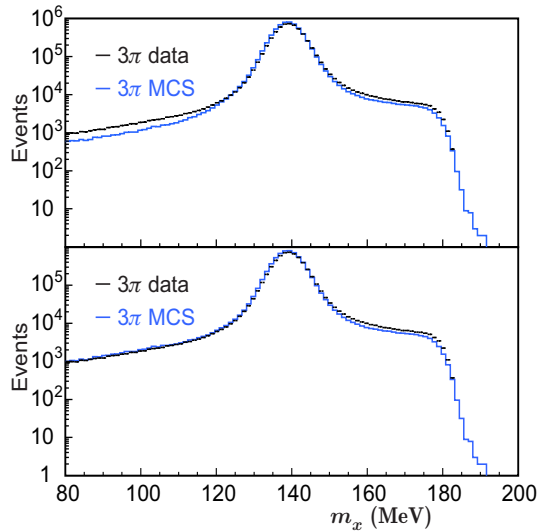

Fig. 4. Data and MC m_x distributions for the $\pi^+\pi^-\pi^0$ control sample, before (upper) and after (lower) resolution correction.

Contributions from $e^+e^- \rightarrow e^+e^-\mu^+\mu^-$ and $e^+e^- \rightarrow e^+e^-\pi^+\pi^-$ processes are evaluated using the Nextcalibur [29] and Ekhara [30] MC generators. After analysis cuts, the $e^+e^- \rightarrow e^+e^-\pi^+\pi^-$ process is found to be negligible, while the $e^+e^- \rightarrow e^+e^-\mu^+\mu^-$ background contribution is between 0.6% and 0.1%, in the low $M_{\mu\mu}^2$ region and is subtracted from the data spectrum [23].

Systematic errors in the background subtraction include: (*i*) Errors on the parameters from the fit procedure: these decrease monotonically from 0.7% to 0.1% with respect to s_μ; (*ii*) The uncertainty on the data/MC resolution

corrections: about 1% in the ρ mass region, smaller at higher s_μ, negligible at lower s_μ values; (*iii*) The uncertainty on the $e^+e^- \to e^+e^-\mu^+\mu^-$ process: about 0.4% at low s_μ values, rapidly falling to 0.1% for $s_\mu > 0.5$ GeV^2. The correctness of the background estimate has been checked by two independent methods.

(1) We perform a kinematic fit of the two track events assuming it is a $\mu\mu\gamma$ state. The χ^2 value obtained is used as discriminant variable, instead of m_x, in the fitting procedure described above.
(2) We improve the π-μ separation by use of m_x, applying a quality cut on the helix fit for both tracks. This cut reduces the dipion background in the dimuon signal region by more than a factor of two.

The background fractions obtained for both cases are in good agreement with the standard procedure [23].

3.4 Efficiencies, acceptance and systematic errors

The MC generator `Phokhara`, including next-to-leading-order ISR as well as FSR corrections [21] has been inserted in the standard KLOE MC `Geanfi` [31]. We compared MC efficiencies with efficiencies obtained from data control samples, and studied two major effects: the EMC response to muons clusters and the muon DC tracking efficiency.

EMC response. From a subsample of $\mu\mu\gamma$ events with both tracks fitted, the efficiency to find at least a cluster with $L > 0$ is found to be equal to one within 10^{-4}. The trigger efficiency is obtained from a sample of $\mu\mu\gamma$ events where a single muon satisfies the trigger requirements. Then, the trigger response for the other muon is parametrized as a function of its momentum and direction. The efficiency as function of s_μ is obtained using the MC event distribution and is equal to one within $5 \cdot 10^{-4}$.

Tracking. Using one muon to tag the presence of the other we find that the tracking efficiency is about 99%, almost constant in s_μ. The systematic error is evaluated varying the purity of the control sample and ranges from 0.3 to 0.6%.

Acceptance and m_x. Efficiencies for m_x cuts and acceptance are evaluated from MC, corrected to reproduce data distributions. The systematic uncertainty due to the m_x cut is obtained by moving the cut by about one sigma of the mass resolution and evaluating the difference in the $\mu\mu\gamma$ spectrum. We find a fractional difference of 0.4% (constant in s_μ) which we take as systematic error. Systematic effects due to polar angle requirements for the muons, $50° < \theta < 130°$, and of dimuon, $|\cos\theta_{\mu\mu}| > \cos(15°)$, are estimated by varying

9

the angular acceptance by 1° (more than two times the resolution on the polar angle of the muon tracks) around the nominal value. The systematic error ranges from 0.1 to 0.6%.

4 Results

4.1 Evaluation of $\sigma(e^+ e^- \to \mu^+ \mu^- \gamma)$ and comparison with QED at NLO

The differential $\mu^+\mu^-\gamma$ cross section is obtained from the observed event count N_{obs} and background estimate N_{bkg}, as

$$\frac{\mathrm{d}\sigma_{\mu\mu\gamma}}{\mathrm{d}s_\mu} = \frac{N_{\mathrm{obs}} - N_{\mathrm{bkg}}}{\Delta s_\mu} \frac{1}{\epsilon(s_\mu)\,\mathcal{L}}. \tag{5}$$

where $\mathcal{L}$ is the integrated luminosity from Ref. 32 and $\epsilon(s_\mu)$ the selection efficiency. Figure 5 top, shows the measured $\mu^+\mu^-\gamma$ cross section compared
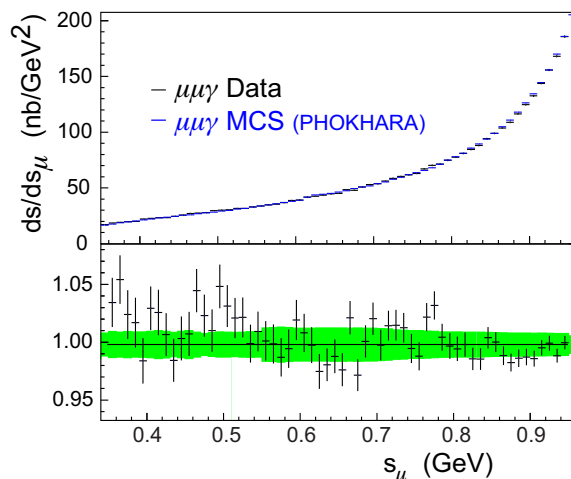

Fig. 5. Top. Comparison of data and MC results for $\mathrm{d}\sigma_{\mu\mu\gamma}/\mathrm{d}s_\mu$. Bottom. Ratio of the two spectra. The green band shows the systematic error.

with the QED calculations to NLO, using the MC code Phokhara [21]. Figure 5 bottom, shows the ratio between the two differential cross sections. The green band indicates the systematic uncertainty, experimental and theoretical, of the measured cross section. The average ratio, using only statistical errors, is 0.9981 ± 0.0015, showing a good agreement within the quoted systematic uncertainties.

4.2 Determination of $\sigma(e^+e^- \to \pi^+\pi^-(\gamma))$ from the $\pi^+\pi^-\gamma/\mu^+\mu^-\gamma$ ratio.

From the bin-by-bin ratio between our published [15] $\pi^+\pi^-\gamma$ and the $\mu^+\mu^-\gamma$ differential cross sections described above, we obtain the bare cross section $\sigma^0_{\pi\pi(\gamma)}$ (inclusive of FSR, with VP effects removed) which is used in the dispersion integral for computing $\Delta^{\pi\pi}a_\mu$. Figure 6 shows the $\pi^+\pi^-\gamma$ and $\mu^+\mu^-\gamma$ event spectra after background subtraction and data/MC corrections. Figure 7
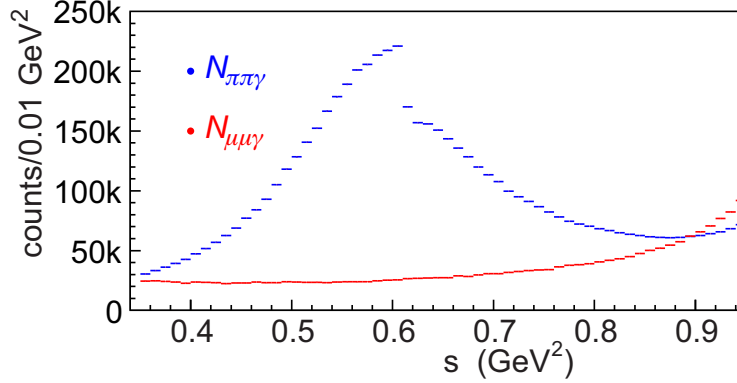

Fig. 6. Square invariant mass distributions of $\pi^+\pi^-\gamma$ (blue) and $\mu^+\mu^-\gamma$ (red) events after background subtraction and data/MC corrections.

shows the bare cross section $\sigma^0_{\pi\pi(\gamma)}$. The pion form factor $|F_\pi|^2$ is then obtained
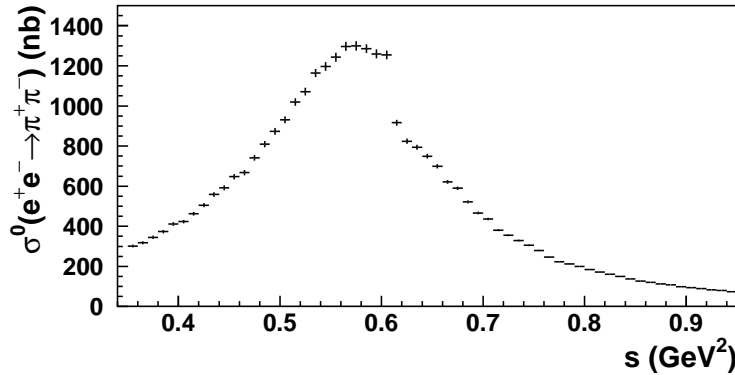

Fig. 7. The bare cross section from the $\pi^+\pi^-\gamma/\mu^+\mu^-\gamma$ ratio.

using Eq. 4.

Table 3 gives our results for the bare cross section and the pion form factor. Only statistical errors are shown. Systematic uncertainties on $\sigma^0_{\pi\pi(\gamma)}$ and $|F_\pi|^2$ are given in Ref. 23. Most of them are smaller than the individual uncertainty on $\pi\pi\gamma$ and $\mu\mu\gamma$ due to correlation between the two measurements [23].

5 Evaluation of $\Delta^{\pi\pi}a_\mu$ and comparisons with other KLOE results

The dispersion integral for $\Delta^{\pi\pi}a_\mu$ is computed as the sum of the values for $\sigma^0_{\pi\pi(\gamma)}$ listed in Table 3 times the kernel $K(s)$, times $\Delta s = 0.01$ GeV^2 :

$$\Delta^{\pi\pi}a_\mu = \frac{1}{4\pi^3} \int\limits_{s_{min}}^{s_{max}} \mathrm{d}s\, \sigma^0_{\pi\pi(\gamma)}(s)\, K(s) \; , \tag{6}$$

where the kernel is given in in Ref. 13. Equation 6 gives $\Delta^{\pi\pi}a_\mu = (385.1 \pm 1.1_{\mathrm{stat}} \pm 2.6_{\mathrm{exp}} \pm 0.8_{\mathrm{th}}) \times 10^{-10}$ in the interval $0.35 < M^2_{\pi\pi} < 0.95$ GeV^2. For each bin contributing to the integral, statistical errors are combined in quadrature and systematic errors are added linearly. Contributions to the $\Delta^{\pi\pi}a_\mu$ systematic uncertainty are shown in Table 1. It is worth emphasizing

Systematic sources	$\Delta^{\pi\pi}a_\mu$
Background subtraction	0.6%
m_x acceptance	0.2%
PID	negligible
Tracking	0.1%
Trigger	0.1%
Geometrical acceptance	negligible
Unfolding	negligible
Software Trigger	0.1%
Experimental systematics	0.7%
Vacuum Polarization	negligible
FSR correction	0.2%
Theory systematics	0.2%
Total systematic error	0.7%

Table 1
List of systematic errors on the $\Delta^{\pi\pi}a_\mu$ measurement. Many systematic effects on the individual $\pi\pi\gamma$ and $\mu\mu\gamma$ analyses cancel in the ratio.

that the use of the $\pi\pi\gamma$ to $\mu\mu\gamma$ ratio results in a reduction of the systematic error compared with that published [15] due to correlations between the $\pi\pi\gamma$ and $\mu\mu\gamma$ measurements and almost negligible theoretical uncertainty.

Figure 8 (top) shows the comparison between the present $|F_\pi|^2$ measurement and the previous KLOE [14] measurement, requiring the ISR photon to be reconstructed at large angle, inside the EMC barrel. Figure 8 (down) shows the fractional difference between the two measurements. They are done on independent data sets, with different running conditions ($W = M_\phi$ here, $W = 1$ GeV in Ref. 14), and also with a different selection, that in turn imply independent systematic uncertainties. The two measurements are in very good agreement.
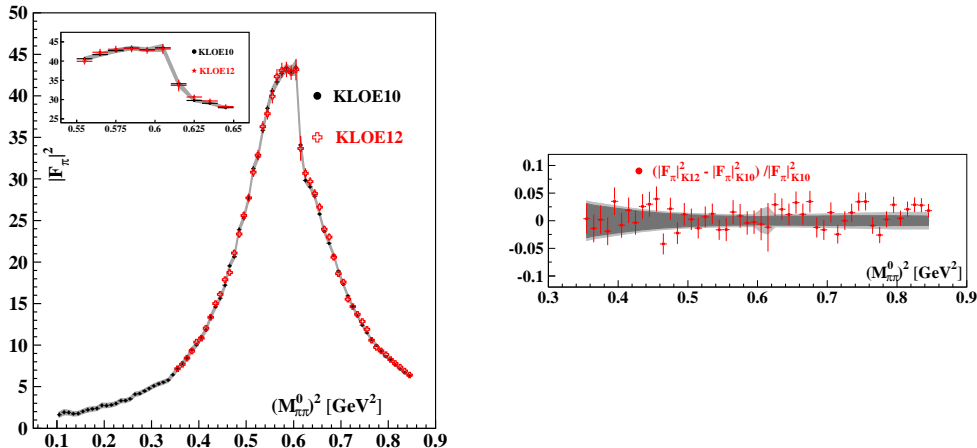
Fig. 8. Left: the pion form factor obtained in this work, KLOE12 (crosses) and from the measurement with the photon at large angle, KLOE10 [14] (points). Right: fractional difference between the two $|F_\pi|^2$ measurements. The dark grey band is the statistical error from [14], the light grey band is the combined statistical and systematic uncertainty. In both figures, errors on crosses include combined statistical and systematic uncertainties.

Table 2 summarizes the comparison between the two most recent KLOE published measurements and the present work on $\Delta^{\pi\pi}a_\mu$: the three results are in very good agreement.

Measurement	$\Delta^{\pi\pi}a_\mu[0.35 - 0.85 \text{ GeV}^2] \times 10^{10}$
this work	$377.4 \pm 1.1_{\text{stat}} \pm 2.7_{\text{sys\&theo}}$
large γ angle [14]	$376.6 \pm 0.9_{\text{stat}} \pm 3.3_{\text{sys\&theo}}$
	$\Delta^{\pi\pi}a_\mu[0.35 - 0.95 \text{ GeV}^2] \times 10^{10}$
this work	$385.1 \pm 1.1_{\text{stat}} \pm 2.7_{\text{sys\&theo}}$
small γ angle [15]	$387.2 \pm 0.5_{\text{stat}} \pm 3.3_{\text{sys\&theo}}$

Table 2
Comparison on $\Delta^{\pi\pi}a_\mu$ between our most recent measurements and the present work.

6 Conclusions

We have measured the differential cross section $\mathrm{d}\sigma(e^+e^- \to \mu^+\mu^-\gamma)/\mathrm{d}M^2_{\mu\mu}$ using events with initial state radiation photons emitted at small angle and inclusive of final state radiation. The measurement is in good agreement with QED to NLO prediction. We determined the pion form factor from the ratio between the $\mathrm{d}\sigma(e^+e^- \to \pi^+\pi^-\gamma)/\mathrm{d}M^2_{\pi\pi}$ and $\mathrm{d}\sigma(e^+e^- \to \mu^+\mu^-\gamma)/\mathrm{d}M^2_{\mu\mu}$ cross sections, measured with the same data set. In this way, the radiator H function

$M^2_{\pi\pi}$ GeV^2	$\sigma^0_{\pi\pi(\gamma)}$ nb	$|F_\pi|^2$	$M^2_{\pi\pi}$ GeV^2	$\sigma^0_{\pi\pi(\gamma)}$ nb	$|F_\pi|^2$
0.355	302±8	7.16±0.18	0.655	699±11	26.62±0.41
0.365	319±8	7.68±0.19	0.665	621±9	23.96±0.36
0.375	345±8	8.45±0.20	0.675	590±9	23.01±0.35
0.385	373±9	9.28±0.22	0.685	522±8	20.59±0.31
0.395	411±9	10.38±0.24	0.695	466±7	18.60±0.27
0.405	423±9	10.85±0.23	0.705	436±6	17.58±0.25
0.415	463±10	12.05±0.26	0.715	381±5	15.53±0.21
0.425	505±10	13.35±0.27	0.725	355±5	14.64±0.21
0.435	559±12	14.99±0.31	0.735	329±4	13.72±0.19
0.445	591±12	16.11±0.33	0.745	305±4	12.84±0.18
0.455	647±13	17.89±0.37	0.755	279±4	11.89±0.16
0.465	668±13	18.73±0.36	0.765	246±3	10.58±0.14
0.475	741±14	21.09±0.40	0.775	224±3	9.72±0.13
0.485	809±16	23.37±0.45	0.785	212±3	9.30±0.12
0.495	873±17	25.60±0.49	0.795	200±2	8.87±0.11
0.505	932±17	27.72±0.51	0.805	185±2	8.26±0.10
0.515	1020±18	30.82±0.55	0.815	173±2	7.80±0.09
0.525	1071±19	32.87±0.58	0.825	161±2	7.34±0.08
0.535	1165±20	36.28±0.63	0.835	149±2	6.88±0.08
0.545	1197±21	37.86±0.68	0.845	138±2	6.40±0.07
0.555	1243±22	39.94±0.71	0.855	126±1	5.94±0.06
0.565	1297±23	42.33±0.75	0.865	120±1	5.71±0.06
0.575	1300±23	43.08±0.76	0.875	113±1	5.38±0.05
0.585	1285±22	43.19±0.75	0.885	108±1	5.18±0.05
0.595	1260±22	42.83±0.76	0.895	99±1	4.80±0.04
0.605	1254±21	43.15±0.74	0.905	94±1	4.60±0.04
0.615	916±15	33.68±0.55	0.915	89±1	4.39±0.04
0.625	824±13	30.68±0.50	0.925	83±1	4.13±0.03
0.635	794±12	29.68±0.45	0.935	80±1	4.00±0.03
0.645	749±12	28.23±0.44	0.945	74.0±0.5	3.75±0.03

Table 3

Bare cross section and the pion form factor, in 0.01 GeV^2 intervals. The value given in the $M^2_{\pi\pi}$ column indicates the bin center.

is not used, the luminosity of the sample cancels out and the acceptance corrections compensate resulting in an almost negligible systematic error.
This pion form factor determination is in very good agreement with previous KLOE results. We compute the $\pi^+\pi^-$ contribution to the muon anomaly in the interval $0.592 < M_{\pi\pi} < 0.975$ GeV to be:

$$\Delta^{\pi\pi}a_\mu = (385.1 \pm 1.1_{\text{stat}} \pm 2.6_{\text{exp}} \pm 0.8_{\text{th}}) \times 10^{-10}.$$

with an experimental accuracy of 0.7% and a theoretical uncertainty at the 0.2% level.

This result, with comparable total experimental uncertainty and a theoretical error reduced by about 70% with respect to our previous results, confirms the current discrepancy between the standard model prediction and the experimental value of a_μ.

Acknowledgments

References

[1] G. W. Bennett *et al.* [Muon G-2 Collaboration], Phys. Rev. D **73** (2006) 072003.

[2] J. P. Miller, E. de Rafael and B. L. Roberts, Rept. Prog. Phys. **70** (2007) 795.

[3] F. Jegerlehner and A. Nyffeler, Phys. Rept. **477** (2009) 1.

[4] M. Davier, A. Hoecker, B. Malaescu and Z. Zhang, Eur. Phys. J. C **71** (2011) 1515 [Erratum-ibid. C **72** (2012) 1874].

[5] K. Hagiwara *et al.*, J. Phys. G **38** (2011) 085003.

[6] M. Benayoun, P. David, L. DelBuono and F. Jegerlehner, `http://arxiv.org/abs/1210.7184`.

[7] A. Czarnecki and W. J. Marciano, Phys. Rev. D **64** (2001) 013014.

[8] N. Arkani-Hamed *et al.*, Phys. Rev. D **79** (2009) 015014.

[9] M. Pospelov, Phys. Rev. D **80** (2009) 095002.

[10] The New Muon (g - 2) Collaboration, R.M. Carey *et. al.*, see `http://lss.fnal.gov/archive/testproposal/0000/fermilab-proposal-0989.shtml`

[11] J. Imazato, Nucl. Phys. Proc. Suppl. **129** (2004) 81.

[12] C. Bouchiat and L. Michel, J. Phys. Radium **22** (1961) 121.

[13] B. E. Lautrup and E. de Rafael, Nuovo Cimento, **1A** (1971) 238.

[14] F. Ambrosino *et al.* [KLOE Collaboration], Phys. Lett. B **700** (2011) 102.

[15] F. Ambrosino *et al.* [KLOE Collaboration], Phys. Lett. B **670** (2009) 285.

[16] A. Aloisio *et al.* [KLOE Collaboration], Phys. Lett. B **606** (2005) 12.

[17] S. Binner, J. H. Kühn and K. Melnikov, Phys. Lett. B **459** (1999) 279.

[18] G. Rodrigo, H. Czyż, J. H. Kühn and M. Szopa, Eur. Phys. J. C **24** (2002) 71.

[19] H. Czyz, A. Grzelinska, J. H. Kuhn and G. Rodrigo, Eur. Phys. J. C **27** (2003) 563.

[20] H. Czyz, A. Grzelinska, J. H. Kuhn and G. Rodrigo, Eur. Phys. J. C **33** (2004) 333.

[21] H. Czyż, A. Grzelinska, J. H. Kühn, G. Rodrigo, Eur. Phys. J. C **39** (2005) 411.

[22] S. Actis *et al.* [Working Group on Radiative Corrections and Monte Carlo Generators for Low Energies Collaboration], Eur. Phys. J. C **66** (2010) 585.

[23] P. Lukin, et al., KLOE-2 Note K2PD-6, Dec 2012, `http://www.lnf.infn.it/kloe2/tools/getfile.php?doc_fname=K2PD-6.pdf&doc_ftype=docs`

[24] VP correction values kindly provided by Fred Jegerlehner, `http://www-com.physik.hu-berlin.de/~fjeger/alphaQEDn.uu`

[25] J.S. Schwinger, *Particles, Sources and Fields, Vol.3*, Redwood City, USA Addison-Wesley (1989) 99

[26] M. Adinolfi *et al.*, Nucl. Instrum. Meth. A **488** (2002) 51.

[27] M. Adinolfi *et al.*, Nucl. Instrum. Meth. A **482** (2002) 364.

[28] M. Adinolfi *et al.*, Nucl. Instrum. Meth. A **492** (2002) 134.

[29] F. A. Berends, C. G. Papadopoulos and R. Pittau, Comput. Phys. Commun. **136** (2001) 148.

[30] H. Czyż and E. Nowak-Kubat, Phys. Lett. B **634** (2006) 493.

[31] F. Ambrosino *et al.*, Nucl. Instrum. Meth. A **534** (2004) 403.

[32] F. Ambrosino *et al.* [KLOE Collaboration], Eur. Phys. J. C **47** (2006) 589.